Fluid Phase Equilibria 518 (2020) 112627

Contents lists available at ScienceDirect

Fluid Phase Equilibria

journal homepage: www.elsevier.com/locate/fluid

Determination of surface tension and surface thermodynamic properties of nano-ceria by low temperature heat capacity

Zixiang Cui *, Jiaojiao Chen , Yongqiang Xue **, Junzhen Gan , Xinghui Chen , Huijuan Duan , Rong Zhang , Jiayi Liu , Jie Hao

Department of Chemistry, Taiyuan University of Technology, Taiyuan, 030024, PR China

ARTICLE INFO

Article history:
Received 10 January 2020
Received in revised form
26 April 2020
Accepted 28 April 2020
Available online 6 May 2020

Keywords:
Surface tension
Surface thermodynamic properties
Heat capacity
Nano-CeO_2

ABSTRACT

The surface tension and surface thermodynamic properties play a decisive role in research and applications of nano materials, but they are difficult to be determined, as there is no precise method to measure these properties of nano materials. Herein, we derived the relations between the molar surface thermodynamic functions, surface heat capacity, and particle size. On this basis, a new low-temperature heat capacity method for determining the surface tension and the surface thermodynamic functions of nano materials was proposed. We measured the low temperature heat capacities of nano-CeO_2 and bulk CeO_2 in temperature range from 1.9 K to 300 K at constant pressure by the Physical Property Measurement System (PPMS). The surface tensions and corresponding temperature coefficients of nano-CeO_2 were calculated at different temperatures, and then the surface thermodynamic functions were obtained. The results show that the molar heat capacities of nano-CeO_2 are greater than that of the corresponding bulk CeO_2 in temperature range from 1.9 K to 300 K. The molar surface enthalpy and molar surface entropy of nano-CeO_2 increase with the increase of temperature, while surface tension, temperature coefficient, and molar surface Gibbs energy decrease with the increase of temperature. The proposed low temperature heat capacity method can not only accurately measure surface tension, temperature coefficient, and surface thermodynamic functions of nanoparticles at different temperatures, it also provides a reliable and an accurate experimental method for solving the thermodynamic problems of nanoparticles.

1. Introduction

The surface effects result in the peculiar physical and chemical properties of nano materials [1]. In order to illustrate the influence of surface effects on the physical and chemical properties of nano materials in various processes, a variety of nano-physical chemistry theories have been proposed, such as the thermodynamic theory of nanoparticles [2–4], nano reaction kinetic theory [5–9], nano phase transition theory [10–12], thermodynamic adsorption theory, and others [13,14]. In these theoretical equations describing the surface effects of nano materials in various processes, both the surface thermodynamic properties and the surface tension (or interfacial tension) are included. These equations also show that the surface thermodynamic properties are related to the surface tension. Therefore, the mechanism and influence of the surface effects can be clarified, and all nano thermodynamic theories can be applied accurately, once the problem of surface tension measurement is solved.

Some studies have recently been reported on the surface tension of nanoparticles, however, most of them mainly focused on the theoretical aspect [15,16] and simulation calculation [17]. The experimental determinations of surface tension are rarely reported. Zhang et al. [2] obtained the surface tension of nanoparticles by measuring their solubility in water at different temperatures. However, the surface tension they got was actually the interfacial tension between the nanoparticles and the water, rather than the surface tension between the nanoparticles and the gas. Cuenot et al. [18] measured the surface tension of nano-Ag and nano-Pb by atomic force microscopy, but this method has poorly repeatability and large measurement error [19]. At present, the problem of determining surface tension of nanoparticles needs urgent attention. Therefore, it is necessary to find an accurate and a reliable

* Corresponding author.
** Corresponding author.
E-mail addresses: czxlw2018@163.com (Z. Cui), xyqlw@126.com (Y. Xue).

https://doi.org/10.1016/j.fluid.2020.112627
0378-3812/

method to measure the surface tension and surface thermodynamic properties of nanoparticles.

Nano-CeO_2 is widely used in adsorption, catalysis, photocatalysis, and other fields [20,21], which are related to the surface thermodynamic properties of nano-CeO_2. Measuring the surface tension of nano-CeO_2 would be helpful to analyze various surface processes of nano-CeO_2. In this paper, the relations between the molar surface thermodynamic functions, surface heat capacity, and particle size was derived theoretically. Experimentally, a new method was used to measure the heat capacity of nano-CeO_2 and bulk CeO_2 in temperature range from 1.9 K to 300 K. The surface tension and temperature coefficient of nano-CeO_2 were calculated using heat capacity data, and then the molar surface enthalpy, molar surface entropy, and molar surface Gibbs energy of nano-CeO_2 were obtained.

2. Theory

2.1. Surface thermodynamics of nanoparticles

The Gibbs energy of the nanoparticles can be expressed as follows [2,22],

$$G = G^{b} + G^{s} = G^{b} + \sigma A \tag{1}$$

where G^s and $G^b$are respectively the surface Gibbs energy and the Gibbs energy of the corresponding bulk materials; σ and A are respectively the surface tension and the total surface area of nanoparticles.

For spherical nanoparticles, the surface Gibbs energy can be reduced to

$$G^{s}_{m} = \sigma A_{m} = \frac{3\sigma V_{m}}{r} \tag{2}$$

where V_m and $r$are the molar volume and the radius of nanoparticles, respectively.

By substituting Eq. (2) into the Gibbs-Helmholtz equation$[\partial(G/T)/\partial T]_p = -H/T^2$, the molar surface enthalpy H^s_m can be obtained,

$$H^{s}_{m} = \frac{3\sigma V_{m}}{r}\left[1 - \frac{T}{\sigma}\left(\frac{\partial\sigma}{\partial T}\right)_{p} - \frac{2}{3}T\alpha\right] \tag{3}$$

where $\alpha = (\partial V/\partial T)_p/V$ is the coefficient of volume expansion.

Similarly, the molar surface entropy S^s_m can be obtained by substituting Eq. (2) into $S = -(\partial G/\partial T)_{p,A,n}$,

$$S^{s}_{m} = -\frac{3\sigma V_{m}}{r}\left[\frac{(\partial\sigma/\partial T)}{\sigma} + \frac{2}{3}\sigma\right] \tag{4}$$

In Eqs. (2)–(4), the magnitude of $(\partial\sigma/\partial T)_p$ is -10^{-4} and is less than zero, the magnitude of α is 10^{-6} and is greater than zero [2]. So, it can be seen from Eqs. (2)–(4) that the surface thermodynamic functions are positive, and the smaller the particle size is, the greater the surface thermodynamic functions are.

Substituting Eq. (3) into the heat capacity definition$C_{p,m} = (\partial H_m/\partial T)_p$, the expression of molar surface heat capacity $C^s_{p,m}$ at constant pressure is as follows

$$C^{s}_{p,m} = -\frac{V_m T}{r}\left[2\sigma\left(\frac{\partial\alpha}{\partial T}\right)_{p} + \frac{4}{3}\sigma\alpha^2 + 3\left(\frac{\partial^2\sigma}{\partial T^2}\right)_{p} + 4\alpha\left(\frac{\partial\sigma}{\partial T}\right)_{p}\right] \tag{5}$$

Generally, the magnitudes of σV_m, $(\partial\alpha/\partial T)_p$, α, $(\partial^2\sigma/\partial T^2)_p$ and $(\partial\sigma/\partial T)_p$ are 10^{-1}~10^{0}N·m^{-1} [22], 10^{-5}m^3·mol^{-1}, 10^{-9}, 10^{-6} K^{-1} [23], -10^{-6} N·m^{-1}·K^{-2} and -10^{-4} N·m^{-1}·K^{-1}, respectively. In Eq (5), the two items $2\sigma(\partial\alpha/\partial T)_p$ and $4\sigma\alpha^2/3$ can be ignored, and the other two items in the square brackets are negative, so the surface heat capacity increases with particle size decreases.

2.2. The low temperature heat capacity method

We first measured the heat capacity of the nano materials and bulk materials in temperature range from 1.9 K to 300 K. The relation between the heat capacity and temperature in temperature range from 0 K to 300 K was obtained by fitting the heat capacity data.

The molar entropy of nanoparticles (H^{nm}_m) and bulk materials (H^{b}_m) can be derived by the following equations [24–26],

$$H^{nm}_{m}(T) = H^{nm}_{m}(0K) + \int_0^T C^{nm}_{p,m}\mathrm{d}T \tag{6}$$

$$H^{b}_{m}(T) = H^{b}_{m}(0K) + \int_0^T C^{b}_{p,m}\mathrm{d}T \tag{7}$$

Combining Eqs. (6) and (7), the changes of surface enthalpy can be obtained by subtracting the enthalpy changes of the bulk material from that of the nanoparticles as follows,

$$\Delta H_m = H^{nm}_{m}(T) - H^{b}_{m}(T) = \Delta^{nm}_{b}H_m(0K) + \Delta^{T}_{0}H^{s}_{m} \tag{8}$$

where the $\Delta^{nm}_{b}H_m(0K) = H^{nm}_{m}(0K) - H^{b}_{m}(0K)$,

$$\Delta^{T}_{0}H^{s}_{m} = \Delta^{T}_{0}H^{nm}_{m} - \Delta^{T}_{0}H^{b}_{m} = \int_0^T C^{nm}_{p,m}\mathrm{d}T - \int_0^T C^{b}_{p,m}\mathrm{d}T \tag{9}$$

Similarly, the changes of surface entropy and surface Gibbs energy can be obtained,

$$\Delta^{T}_{0}S^{s}_{m} = \Delta^{T}_{0}S^{nm}_{m} - \Delta^{T}_{0}S^{b}_{m} = \int_0^T \frac{C^{nm}_{p,m}}{T}\mathrm{d}T - \int_0^T \frac{C^{b}_{p,m}}{T}\mathrm{d}T \tag{10}$$

$$\Delta^{T}_{0}G^{s}_{m} = \Delta^{T}_{0}H^{s}_{m} - T\Delta^{T}_{0}S^{s}_{m} \tag{11}$$

where superscript nm and b represent the nano materials and the bulk materials, respectively.

The surface Gibbs energy change $\Delta^{T}_{0}G^{s}_{m}$ is expressed as follows,

$$\Delta^{T}_{0}G^{s}_{m} = \Delta^{T}_{0}(\sigma A_m) \tag{12}$$

and hence the surface Gibbs energy change $\Delta^{T_n}_{T_{n-1}}G^{s}_{m}$ of the temperature change process from T_{n-1} to T_n can be expressed as follows,

$$\Delta^{T_n}_{T_{n-1}}G^{s}_{m} = \Delta^{T_n}_{0}G^{s}_{m} - \Delta^{T_{n-1}}_{0}G^{s}_{m} = (\sigma_{T_n}A_{T_n}) - (\sigma_{T_{n-1}}A_{T_{n-1}}) \tag{13}$$

Since the expansion coefficient α of the solid is small, the surface area in the temperature range T_n to T_{n-1} can be considered as a constant if the temperature change $(T_n - T_{n-1})$ is also small, so Eq. (14) can be obtained,

$$\frac{\Delta^{T_n}_{T_{n-1}}G^{s}_{m}}{A_{m,T_n}} = (\sigma_{T_n} - \sigma_{T_{n-1}}) \tag{14}$$

We can get the $(\partial\sigma/\partial T)_{p,T_n}$ by dividing Eq. (14) by the temperature change $\Delta^{n}_{n-1}T$,

$$\frac{\Delta_{T_{n-1}}^{T_n} G_m^s}{A_{m,T_n} \Delta_{n-1}^n T} = \frac{(\sigma_{T_n} - \sigma_{T_{n-1}})}{\Delta_{n-1}^n T} \approx \left(\frac{\partial \sigma}{\partial T}\right)_{p,T_n} \quad (15)$$

where the $\Delta_{n-1}^n T = T_n - T_{n-1}$.

However, if the temperature changes, the radius of the nanoparticles r, density ρ and molar surface area A_m will also change accordingly. In order to ensure the accuracy and reliability of data processing, the surface area in the one temperature interval is regarded as a constant when calculating Eqs. (14) and (15). The surface area of nanoparticles at different temperature intervals can be calculated by the expansion coefficient.

After getting the temperature coefficient at T_n, for a temperature interval from T_{n-1} to T_n, there is

$$\sigma_{T_{n-1}} \approx \sigma_{T_n} - (\partial \sigma / \partial T)_{p,T_n} \Delta_{n-1}^n T \quad (16)$$

The surface tension at T_n can be obtained by substituting Eq (16) into Eq. (13) as follows,

$$\sigma_{T_n} = \frac{\Delta_{T_{n-1}}^{T_n} G_m^s - A_{m,T_{n-1}} (\partial \sigma / \partial T)_{p,T_n} \Delta_{n-1}^n T}{A_{m,T_n} - A_{m,T_{n-1}}} \quad (17)$$

After obtaining the surface tension and temperature coefficient, the surface enthalpy, surface entropy and Gibbs energy of nanoparticles at different temperatures can be obtained by Eqs. (2)–(4).

The adsorption of water on the surface of nanoparticles has been known as an unavoidable situation caused by the surface effects of nanoparticles. The surface effects of nanoparticles are resulted from the increase of the proportion of surface atoms to the total number of atoms. The smaller is the size of nanoparticles, the greater will be the specific surface area, the greater the surface energy and the more unstable the nanoparticles are. The hydration on surface of nanoparticles can reduce surface tension and surface energy [27,28], which consequentially enhances the stability of the nanoparticles. In consequence, the hydration will decrease the surface thermodynamic properties. On this condition, this situation have been taken into consideration in theoretical derivation and experimental research. The formula above and the following experimental method are both universally applied to the case of water or no water on the surface of nanoparticles.

3. Experimental details

3.1. Experiment reagent

During the course of this study, all the materials used are analytically pure without further purification, as shown in Table 1.

3.2. Preparation and characterization of nano-CeO_2 and bulk CeO_2

Nano-CeO_2 and bulk CeO_2 were prepared by hydrothermal method. First, 6.5 g of $Ce(NO_3)_3 \cdot 6H_2O$ (Aladdin)was dissolved in 30 mL distilled water at room temperature and then added 30 mL of 2.5% aqueous ammonia dropwise for the stirring. Then added 90 mL distilled water to the above solution and obtained brown suspension. The brown suspension was transferenced to a 200 ml sealed Teflon-lined autoclave and heated to 200 °C for 24 h. After a Natural cooling to the room temperature, the precursor powder was collected by centrifugation. Then wash it several times with DI water and ethanol. Next the precursor powder was dried in air for a while, and calcined in air at 400 °C for 2 h. Finally, the nano-CeO_2 was obtained in muff furnace with a heating rate of 3 °C/min. Nano-CeO_2 can be converted into bulk CeO_2 in virtue of directional crystallization on nano-CeO_2 surface using crystal seed method. However, the nano-CeO_2 sample does not change into that of bulk CeO_2 during the heat capacity measurement. The bulk CeO_2 was prepared in virtue of adding nano-CeO_2 to the hydrothermal reaction system for repeated hydrothermal reactions. As you can see from the TG diagram(Fig. S1), all the $Ce(OH)_x$ in the precursor can be completely converted into CeO_2 by calcination at 400 °C. Fig. 1 shows the XRD pattern of the prepared CeO_2 sample, and it can be seen from Fig. 1 that the diffraction peaks have a good match with cubic fluorite CeO_2 (JCPDS 34–0394). The diffraction peaks is very sharp and there are no other impurity peaks. Therefore, the prepared sample has high purity and crystallinity. According to the Scheler equation, the average diameter of the nano-CeO_2 sample was calculated to be 13.4 nm.

The SEM photographs of samples are shown in Fig. 2. As can be seen from Fig. 2a, the morphology of nano-CeO_2 is nearly spherical and the sizes are consistent with the results calculated by Scherrer formula. The XPS characterization was also performed on the nano-CeO_2 and bulk CeO_2 (Fig. S2), the results show that the Ce(IV)/Ce(III) of nano-CeO_2 and bulk CeO_2 are respectively 12.05 and 13.76, and Ce/O of nano-CeO_2 and bulk CeO_2 are respectively 0.546 and 0.537. Therefore, the composition of the nano-CeO_2 and bulk CeO_2 is basically the same, Apart from the surface effects, there is no other difference between nano-CeO_2 and bulk CeO_2.

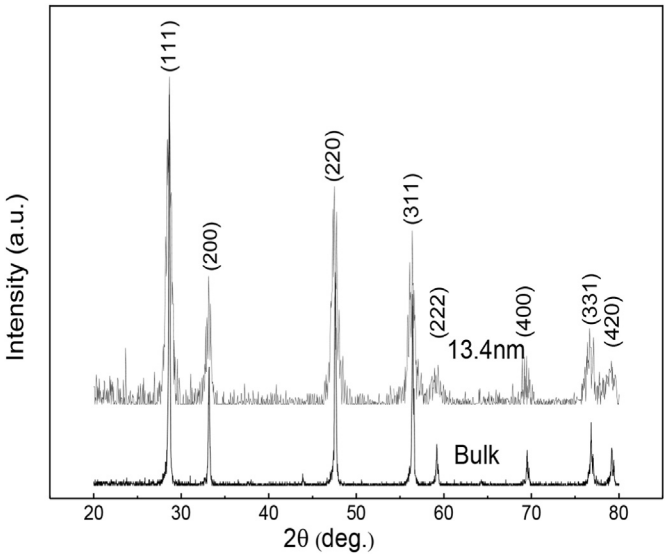

Fig. 1. The XRD patterns of 13.4 nm and bulk CeO_2.

Table 1
Chemical sample description.

component	Molecular formula	Source	Purity (wt.%)[a]
Cerium(III) nitrate	$Ce(NO_3)_3 \cdot 6H_2O$	Aladdin	≥0.99
Ammonium hydroxide	$NH_3 \cdot H_2O$	Beijing huateng chemical co. Ltd., China	0.25
ethanol	CH_3CH_2OH	Tianjin fengchuan chemical reagent technology co. Ltd., China	≥0.99

[a] According to the suppliers.

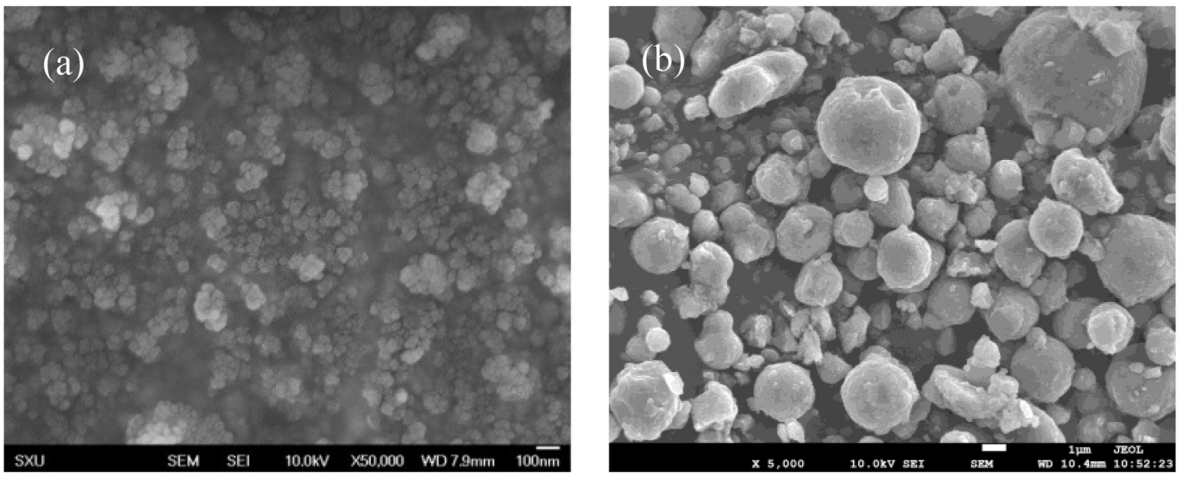

Fig. 2. The SEM images of samples, containing 13.4 nm CeO_2 (a) and bulk CeO_2 (b).

3.3. Heat capacity measurement

The measurement to the heat capacity of the nano-CeO_2 and bulk CeO_2 in the temperature range from 1.9 K to 300 K was conducted by Physical Property Measurement System (PPMS). The PPMS refers to an instrument which was developed by Quantum Design Company of America. The company works to explore the various physical properties of materials. The heat capacity of a small number of samples can be automatically measured in the temperature range of 1.9 K−400 K and the variable magnetic field range of 9 T. The PPMS applies the relaxation method and the adiabatic method to measuring the heat capacity of samples. The system maintains a high vacuum during the measurement, and the top of the sample is also equipped with a heat shield, which can effectively prevent heat loss via convection and radiation. Moreover, the PPMS system has an automatic calibration program and built-in background heat elimination, which ensures more accurate measurement result. Lashley et al. [29] and Kennedy et al. [30] provided details of many instruments and data analysis so that readers can refer to their essays for more information. In this experiment, the selected temperature for measuring the heat capacity of nano-CeO_2 and bulk CeO_2 was 1.9 K−300 K, and the magnetic field was set to 0. The CeO_2 powder has a low thermal conductivity, hence, the Apezon N grease (M&I Materials LTD, UK) was mixed with 10 mg of samples and placed them in a small copper cup(Alfa Aesar copper foil, 99.999%, 0.025 mm thick). The copper cup can be made by ourselves, and then the mixture was compressed with a stainless steel die, so that the heat capacity can be measured on the PPMS heat capacity test platform. The PPMS software, which can subtract the heat capacity of addenda under the sample measurement temperature, is able to automatically calculate the heat capacity of nano-CeO_2 and bulk CeO_2. The addition of the Apezon N grease helped realize better thermal contact between the platform and the sample disc. The PPMS method described above, which can expresses effectiveness and feasibility, can be also verified by the measurement of the heat capacity of copper powder samples (99.999%, Alfa Aesar) as a temperature function. The accuracy of measuring heat capacity is determined by measuring the heat capacity of high purity copper pellet of the standard material. The accuracy is respectively ±2% below 20 K and ±0.6% above 20 K. During the determination of powder samples, a technique discussed by Shi et al. [31] was used to measure the powder samples with an accuracy of ±2% below 20 K and ±1% above 20 K respectively.

4. Results and discussion

4.1. Results of heat capacity measurement

The molar heat capacity datas of nano-CeO_2 and bulk CeO_2 measured by PPMS calorimeter are shown in Fig. 3, and the inset shows the same datas in a limited temperature range below 15 K. The detailed experimental datas are listed in Table S1.

It can be clearly seen from Fig. 3 that the heat capacity curves of nano-CeO_2 and bulk CeO_2 are smooth and there is no anomalies such as phase change in the temperature range from 1.9 K to 300 K. The heat capacity of nano-CeO_2 and bulk CeO_2 increase with the increase of temperature, which is consistent with the experimental result in the literature [32]. In addition, the heat capacity of the bulk CeO_2 is in good agreement with that of the bulk CeO_2 in the literature [33].

When the temperature is lower than 10 K, the heat capacity increases slowly with the increase of temperature, and when it is higher than 50 K, the heat capacity increases rapidly with the increase of temperature, while the increase of the heat capacity of

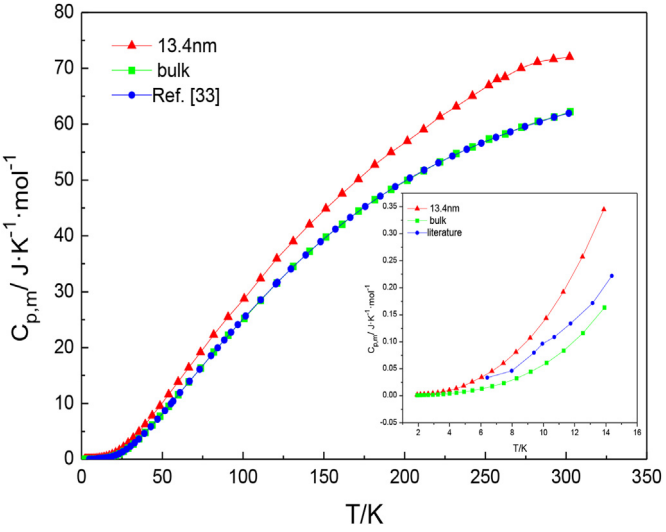

Fig. 3. Molar heat capacity of nano (red) and the bulk (green) CeO_2 from 1.9 K to 300 K. The inset shows the same data for T < 15 K.

nano-CeO2 slowly above 270 K. The difference between the heat capacity of nano-CeO_2 and bulk CeO_2 is the surface heat capacity of nano-CeO_2 ($C^{s}_{p,m} = C^{nm}_{p,m} - C^{b}_{p,m}$). The surface heat capacity of nano-CeO_2 is very small below 10 K and increases with temperature. When the temperature reaches about 270 K, the surface heat capacity reaches its maximum.

In addition, Fig. 3 explicitly showed that the heat capacity of nano-CeO_2 is greater than that of bulk CeO_2, which is because of the high specific surface area and strong quantum size effect of nano-CeO_2. Therefore, the thermodynamic properties of nano-CeO_2 are different from those of bulk CeO_2. The differentiation lies in the surface energy term. Specifically, the contribution of the surface energy term will enhance with the growth of the specific surface area. The higher the specific surface area is, the greater the surface enthalpy is and the higher the energy of nano-CeO_2 is [34]. At the same temperature, the energy of nano-CeO_2($dH = C_p dT$) is higher than that of bulk CeO_2, so the heat capacity of nano-CeO_2 is larger.

In order to carry out a detailed discussion and obtain accurate data to calculate the change of thermodynamic functions, the temperature rang from 1.9 K to 300 K was subdivided into three suitable temperature intervals, and the heat capacity was fitted.

When the temperature is higher than 10 K, the resulting heat capacity can be described by the three theoretical functions of lattice vibration, electron and magnetic contribution. The relationship between the electron contribution and temperature T is linear, and in order to describe the contribution of the lattice, the odd-power series in T is generally used to represent the oxides of CeO_2 without considering the magnetic contribution [35–38]:

$$C_{p,m} = \gamma T + B_3 T^3 + B_5 T^5 \quad (18)$$

For low temperature heat capacity, the linear term γT plays a very important role. The properties of different materials are different, so the contribution of the linear term γT to the heat capacity is also different. There are other odd powers in Eq. (18), which represent the harmonic lattice model. When the temperature is greater than 15 K, the lattice vibration is the main contribution to the heat capacity, so the Debye function and the Einstein function are combined to express it. The heat capacity datas less than 1.9 K can be obtained by extrapolating from Eq. (18). The fitting parameters below 10 K are listed in Table 2.

As can be seen from Table 2, the electronic contribution of the heat capacity in the whole is still significant in the very low temperature range (0 K–3 K). When the temperature increases, the lattice contribution becomes the dominant factor. It can be seen from Fig. 3 that the difference of heat capacity between nano-CeO_2 and bulk CeO_2 is more obvious at higher temperature, and the main contribution is the difference of lattice contribution between the nano-CeO_2 and bulk CeO_2. Because of the high proportion of the total number of atoms on the surface of the nanoparticles, the surface effect is very strong, so the surface tension and surface energy are higher than those of the corresponding bulk materials. Under the action of the surface tension of nanoparticles, it can produce elastic deformation and lattice contraction. The smaller the nanoparticles are, the larger the lattice shrinkage will be [39].

Table 2
The fit parameters for $C_{p,m}$ at constant pressure (p = 0.10 MPa) for nano-CeO_2 and bulk CeO_2 from 2 K to 10 K[a].

Parameters	[b]13.4 nm	[c]Bulk
γ/J·mol^{-1}·K^{-2}	5.0372e-04	1.5413e-04
B_3/J·mol^{-1}·K^{-4}	1.3587e-04	5.0924e-05
B_5/J·mol^{-1}·K^{-6}	4.0449e-08	5.1726e-08
RMS%	3.7722	3.1663

[a] u(T) = ± 0.01 K and u(p) = ± 0.05 kPa.
[b] u(l) = ± 1.0 nm.
[c] u(l) = ± 0.5 μm.

Table 3
The fitting parameters for heat capacity datas at constant pressure (p = 0.10 MPa) for nano-CeO_2 and bulk CeO_2 from 10 K to 50 K[a].

Parameters	[b]13.4 nm	[c]Bulk
A_0/J·mol^{-1}·K^{-1}	−0.43810	−0.61770
A_1/J·mol^{-1}·K^{-2}	0.13250	0.17360
A_2/J·mol^{-1}·K^{-3}	−0.01434	−0.01788
A_3/J·mol^{-1}·K^{-4}	8.2100e-04	8.5820e-04
A_4/J·mol^{-1}·K^{-5}	−1.4410e-05	−1.4030e-05
A_5/J·mol^{-1}·K^{-6}	8.7100e-08	8.0740e-08
RMS%	0.77030	0.27070

[a] u(T) = ± 0.01 K and u(p) = ± 0.05 kPa.
[b] u(l) = ± 1.0 nm.
[c] u(l) = ± 0.5 μm.

The heat capacity of the samples in the temperature range from 10 K to 50 K was polynomial fitting [36,40]. The fitting equation is as follows, and the fitting parameters are shown in Table 3.

$$C_{p,m} = A_0 + A_1 T + A_2 T^2 + A_3 T^3 + A_4 T^4 + A_5 T^5 \quad (19)$$

We used the Debye-Einstein equation to fit experimental datas over a temperature range of 50 K as follows,

$$C_{p,m} = nD(\theta_D) + mE(\theta_E) + aT + bT^2 \quad (20)$$

$$D(x) = 9R\left(\frac{1}{x}\right)^3 \int_0^x \frac{x^4 e^x}{(e^x - 1)^2} dx \quad x = \theta_D / T \quad (21)$$

$$E(x) = 3Rx^2 \cdot \frac{e^x}{(e^x - 1)^2} \quad x = \theta_E / T \quad (22)$$

where $D(\theta_D)$ and $E(\theta_E)$ represent the Debye equation and the Einstein equation, respectively; θ_D and θ_E represent the Debye temperature and the Einstein temperature, respectively; m, n, a and b are the adjustment coefficients; R is the ideal gas constant.

The fitting parameters of heat capacity in the temperature range from 50 K to 300 K are shown in Table 4.

As can be seen from Table 4, the Debye temperature of nano-CeO_2 is lower than that of bulk CeO_2, and the heat capacity of nano-CeO_2 is larger than that of the bulk CeO_2. The sum of the coefficients n and m in Eq. (20) is theoretically approximately equal to the atomic number of per unit formula, and the observed value of 2.9 for nano-CeO_2 and 2.6 for bulk are in good agreement with the expected value.

In order to calculate the surface tension and temperature coefficient at different temperatures.

Hayashi et al. [41] calculated the density of CeO_2 at 298 K and the coefficient of thermal expansion of CeO_2 from 100 K to 900 K(Fig. S3). The particle size r, molar surface area A_m and molar volume V_m of the 13.4 nm (298 K) nano-CeO_2 were calculated in temperature range from 100 K to 300 K, and the calculation interval was 1 K. (Fig. S4).

4.2. Surface tension and temperature coefficient of nano-CeO_2

The thermodynamic properties can be obtained by substituting the measured heat capacity datas of nano-CeO_2 and bulk CeO_2 into Eqs. (9)–(11) (Table S2). The results are shown in Fig. 4.

It can be seen from Fig. 4 that the enthalpy change and entropy change of nano-CeO_2 and bulk CeO_2 increase with the increase of

Table 4
The fitting parameters for heat capacity datas at constant pressure ($p = 0.10$ MPa) for nano-CeO_2 and bulk CeO_2 from 50 K to 300 K[a].

Parameters	[b]13.4 nm	[c]Bulk
n/mol	1.3747	1.3134
θ_D/K	271.63	333.37
m/mol	1.6115	1.3597
θ_E/K	539.44	605.39
a/J·mol^{-1}·K^{-2}	−0.0262	0.022840
b J·mol^{-1}·K^{-3}	2.3000e-04	−1.0970e-06
RMS%	0.27279	0.22279

[a] u(T) = ± 0.01 K and u(p) = ± 0.05 kPa.
[b] u(l) = ± 1.0 nm.
[c] u(l) = ± 0.5 μm.

temperature, while the Gibbs energy decreases with the increase of temperature. There is significant difference in thermodynamic properties between nano-CeO_2 and bulk CeO_2. The difference between the change of the thermodynamic functions of nano-CeO_2 and bulk CeO_2 are the change of the molar surface thermodynamic functions (Table S3).

The Gibbs energy change $\Delta_T^{T+1}G_{\mathrm{m}}^{\mathrm{s}}$, (100 K < T < 299 K) of each interval of 1 K were calculated by Eq. (13) in temperature range from 100 K to 300 K. The Gibbs energy change $\Delta_T^{T+1}G_{\mathrm{m}}^{\mathrm{s}}$ and surface area A_{m} at different temperatures were substituted into Eq (14) to calculate the temperature coefficient of nano-CeO_2 in the temperature range from 100 K to 300 K. The result is shown in Fig. 5.

It can be seen from Fig. 5 that the surface tension temperature coefficient of the nano-CeO_2 decreases with the increase of temperature in the range of 100 K—300 K, and is approximately linearly related.

The surface tension of nano-CeO_2 in the temperature range from 100 K to 300 K was calculated by substituting the temperature coefficient $(\partial\sigma/\partial T)_{p,T}$ and the molar surface area A_{m} into Eq. (17). The result is shown in Fig. 6.

As shown in Fig. 6, the surface tension of nano-CeO_2 decreases with the increase of temperature in the temperature range from 100 K to 300 K, which is consistent with the experimental result in the literature [42]. This is because as the temperature rises, the lattice of nanoparticles expands and the force between atoms weakens, causing the surface tension of the nanoparticles to decrease. The influence law is consistent with the bulk materials.

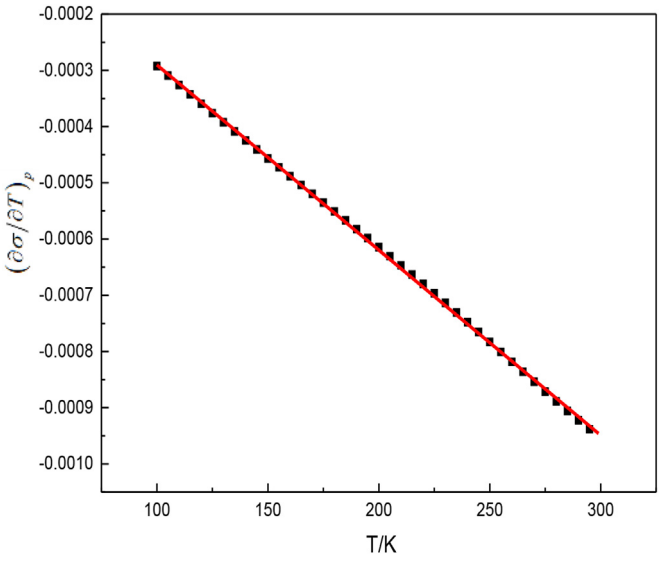

Fig. 5. The temperature coefficient of nano-CeO_2 in the temperature range of 100 K—300 K.

4.3. The surface thermodynamic functions and the surface heat capacity of nano-CeO_2

On the basis of obtaining temperature coefficient and surface tension of nano-CeO_2, the surface enthalpy $H_{\mathrm{m}}^{\mathrm{s}}$, surface entropy $S_{\mathrm{m}}^{\mathrm{s}}$ and surface Gibbs energy $G_{\mathrm{m}}^{\mathrm{s}}$ of nano-CeO_2 can be obtained by Eqs. (2)—(4), respectively. The results are shown in Fig. 7.

Fig. 7 shows that the surface enthalpy and surface entropy of nano-CeO_2 increase with the increase of temperature, while the surface Gibbs energy decreases with the increase of temperature, which is consistent with the experimental results in the literature [43]. This is because the molar surface area increases slowly with the increase of temperature, while the surface tension decreases significantly with the increase of temperature, resulting in the surface Gibbs energy decreases with the increase of temperature.

4.4. Surface heat capacity

The surface heat capacity of nano-CeO_2 is calculated by

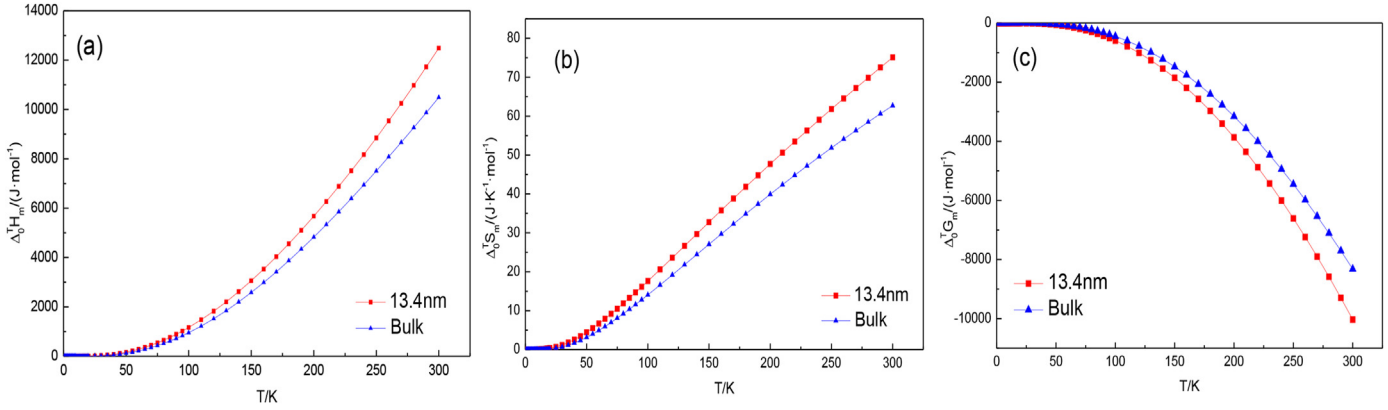

Fig. 4. The thermodynamic changes in (0—300) K of the nano-CeO_2 and bulk CeO_2, containing the molar enthalpy change $\Delta_0^T H_{\mathrm{m}}$(a), the molar entropy change $\Delta_0^T S_{\mathrm{m}}$(b) and the molar Gibbs energy change $\Delta_0^T G_{\mathrm{m}}$(c).

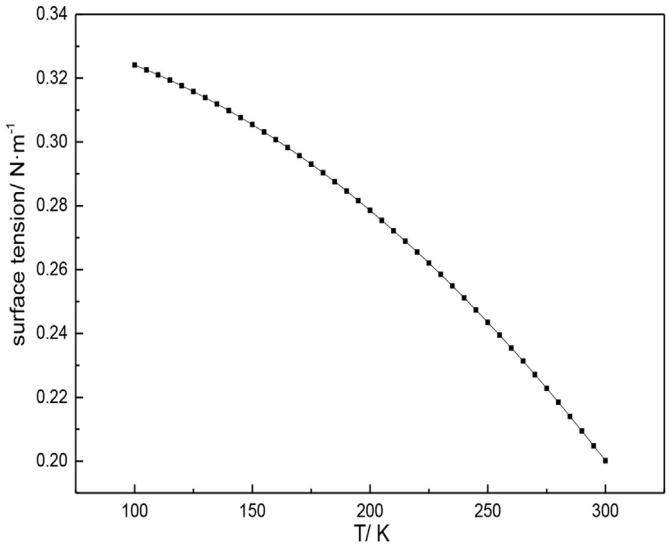

Fig. 6. Plot of the relationship between surface tension and temperature of nano-CeO_2 in the temperature range from 100 K to 300 K.

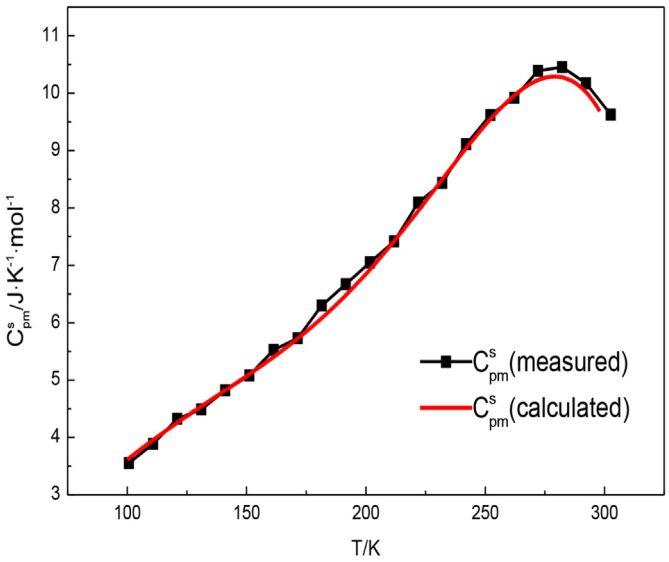

Fig. 8. Comparison of the calculated surface heat capacity and the measured surface heat capacity.

substituting the obtained surface tension and temperature coefficient into Eq. (5), which is called the calculated surface heat capacity (Table S4). The surface heat capacity of nano-CeO_2 determined by experiment, namely the measured surface heat capacity, can also be obtained by subtracting the bulk heat capacity from the heat capacity of nano-CeO_2. The calculated surface heat capacity datas and the measured surface heat capacity datas were plotted together are shown in Fig. 8.

As can be seen from Fig. 8, the calculated surface heat capacity is consistent well with the measured datas, which indicates that the method of measuring surface tension and the temperature coefficient by low temperature heat capacity is reliable. Moreover, it also shows that the relationship between the surface thermodynamic functions and surface heat capacity of nanoparticles is accurate.

5. Conclusions

In this paper, a new method of measuring surface tension and surface thermodynamic functions of nanoparticles is proposed, namely low temperature heat capacity method. In this paper, the low temperature heat capacity of the nano-CeO_2 and bulk CeO_2 in the temperature range from 1.9 K to 300 K was measured by PPMS for the first time, and then obtained the surface tension and surface thermodynamic functions of nano-CeO_2 by the method. The results show that the surface enthalpy and surface entropy of nano-CeO_2 increase with the increase of temperature, and the surface Gibbs energy and the surface tension decrease with the increase of temperature. At a certain constant pressure, the surface heat capacity of nano-CeO_2 tends to rise first and then fall with the increase of temperature. The method proposed can not only accurately measure the surface tension and the surface thermodynamic functions of nanoparticles at different temperatures, but

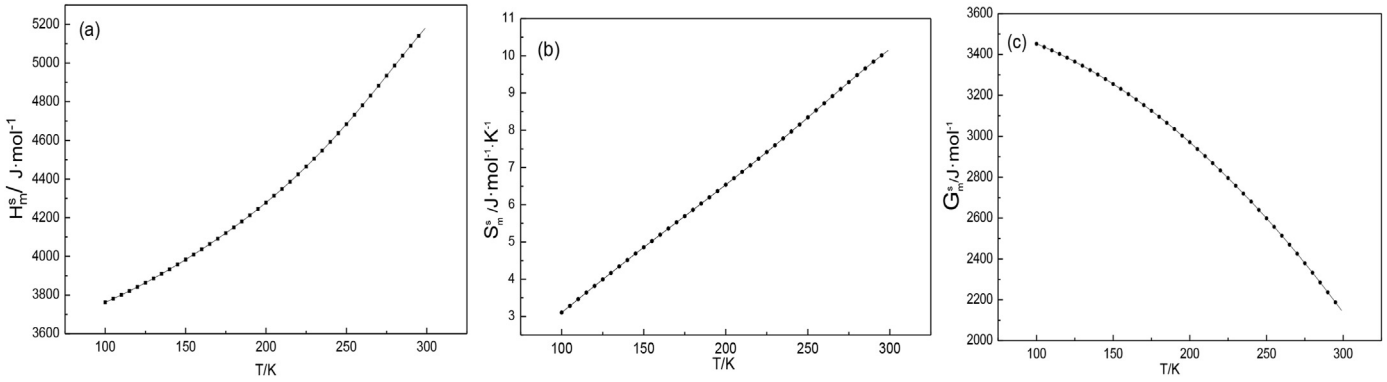

Fig. 7. The surface thermodynamic functions in 100 K–300 K of the nano-CeO_2, containing the molar surface enthalpy H_m^s (a), the molar surface entropy S_m^s (b) and the molar surface Gibbs energy G_m^s (c).

also has important scientific significance and practical significance for the research and application of nano-thermodynamics.

Declaration of competing interest

The authors declare that they have no known competing financial interests or personal relationships that could have appeared to influence the work reported in this paper.

CRediT authorship contribution statement

Zixiang Cui: Conceptualization, Methodology, Investigation, Resources, Supervision, Project administration. **Jiaojiao Chen:** Formal analysis, Data curation, Writing - original draft. **Yongqiang Xue:** Resources, Writing - review & editing, Supervision, Project administration, Funding acquisition. **Junzhen Gan:** Data curation, Investigation. **Xinghui Chen:** Software, Writing - original draft. **Huijuan Duan:** Supervision, Formal analysis. **Rong Zhang:** Investigation, Supervision. **Jiayi Liu:** Visualization, Investigation. **Jie Hao:** Visualization, Investigation.

Acknowledgements

The authors are very grateful for the financial support from the National Natural Science Foundation of China (Nos. 21573157 and 21373147).

Appendix A. Supplementary data

Supplementary data to this article can be found online at https://doi.org/10.1016/j.fluid.2020.112627.

References

[1] P. Ball, L. Garwin, Science at the atomic scale, Nature 355 (1992) 761–764.
[2] Z. Zhang, Q.S. Fu, Y.Q. Xue, Theoretical and experimental researches of size-dependent surface thermodynamic properties of nano-vaterite, J. Phys. Chem. C 120 (2016) 21652–21658.
[3] S.S. Wang, Z.X. Cui, X.Y. Xia, Size-dependent decomposition temperature of nanoparticles: a theoretical and experimental study, Physica B 454 (2014) 175–178.
[4] Q.S. Fu, Z.X. Cui, Y.Q. Xue, Size dependence of the thermal decomposition kinetics of nano-CaC_2O_4:A theoretical and experimental study, Eur. Phys. J. Pluse. 130 (2015) 1–14.
[5] Y.Q. Xue, B.J. Gao, J.F. Gao, The theory of thermodynamics for chemical reactions in dispersed heterogeneous systems, J. Colloid Interface Sci. 191 (1997) 81–85.
[6] Q.S. Fu, Y.Q. Xue, Z.X. Cui, M. Wang, Study on the size-dependent oxidation reaction kinetics of nanosized zinc sulfide, J. Nanomater. 2014 (2014) 1–8.
[7] Z.Y. Huang, X.X. Li, Z.J. Liu, Morphology effect on the kinetic parameters and surface thermodynamic properties of Ag_3PO_4, micro-/nanocrystals, J. Nanomater. 16 (2015), 388–343.
[8] G. F Liao, J. Chen, W.G. Zeng, C.H. Yu, C.F. Yi, Z.S. Xu, Facile preparation of uniform nanocomposite spheres with loading silver nanoparticles on polystyrene-methyl acrylic acid spheres for catalytic reduction of 4-nitrophenol, J. Phys. Chem. C 120 (2016) 25935–25944.
[9] G.F. Liao, Q. Li, W.Z. Zhao, Q.H. Pang, H.Y. Gao, Z.S. Xu, In-situ construction of novel silver nanoparticle decorated polymeric spheres as highly active and stable catalysts for reduction of methylene blue dye, Appl. Catal. A-Gen. 549 (2018) 102–111.
[10] Z.X. Cui, M.Z. Zhao, W.P. Lai, Thermodynamics of size effect on phase Transition temperatures of dispersed phases, J. Phys. Chem. C 115 (2011) 22796–22803.
[11] J.H. Zhu, Q.S. Fu, Y.Q. Xue, Comparison of different models of melting transformation of nanoparticles, J. Mater. Sci. 51 (2016) 4462–4469.
[12] Q.S. Fu, J.H. Zhu, Y.Q. Xue, Size-and shape-dependent melting enthalpy and entropy of nanoparticles, J. Mater. Sci. 52 (2016) 1911–1918.
[13] Y.Z. Wen, Y.Q. Xue, Z.X. Cui, Y.F. Wang, Thermodynamics of nanoadsorption from solution: theoretical and experimental research, J. Chem. Thermodyn. 80 (2015) 112–118.
[14] S.T. Wang, Y.Z. Wen, Z.X. Cui, Size dependence of adsorption kinetics of nano-MgO: a theoretical and experimental study, J. Nano Res. 18 (2016) 1–9.
[15] A. Barnard, L. Curtiss, Computational nano-morphology: modeling shape as well as size, Adv. Mater. Sci. 10 (2005) 105–109.
[16] Y.F. Yang, Y.Q. Xue, Z.X. Cui, Effect of particle size on electrode potential and thermodynamics of nanoparticles electrode in theory and experiment, Electrochim. Acta 136 (2014) 565–571.
[17] M. Farsad, F.J. Vernerey, H.S. Park, An extended finite element/level set method to study surface effects on the mechanical behavior and properties of nanomaterials, Int. J. Numer. Methods Eng. 84 (2010) 1466–1489.
[18] S. Cuenot, C. Frétigny, S. Demoustier-Champagne, Surface tension effect on the mechanical properties of nanomaterials measured by atomic force microscopy, Phys. Rev. B 69 (2004) 1124–1133.
[19] H.J. Butt, B. Cappella, M. Kappl, Force measurements with the atomic force microscope: technique, interpretation and applications, Surf. Sci. Rep. 59 (2005) 1–152.
[20] G.F. Liao, Y. Gong, L. Zhang, H.Y. Gao, G.J. Yang, B.Z. Fang, Semiconductor polymeric graphitic carbon nitride photocatalysts: the “holy grail” for photocatalytic hydrogen evolution reaction under visible light, Energy Environ. Sci. 12 (2019) 2080–2147.
[21] G.F. Liao, J.S. Fang, Q. Li, S.H. Li, Z.S. Xu, B.Z. Fang, Ag-Based nanocomposites: synthesis and applications in catalysis, Nanoscale 11 (2019) 7062–7096.
[22] W.J. Li, Y.Q. Xue, Z.X. Cui, Size dependence of surface thermodynamic properties of nanoparticles and its determination method by reaction rate constant, Physica B 495 (2016) 98–105.
[23] H. Hayashi, M. Kanoh, J.Q. Chang, Thermal expansion of Gd-doped ceria and reduced ceria, Solid State Ionics 132 (2000) 227–233.
[24] A.E. Musikhin, V.N. Naumov, M.A. Bespyatov, The heat capacity of Li_2MoO_4, in the temperature range 6–310 K, J. Alloys Compd. 639 (2015) 145–148.
[25] S. Loos, D. Gruner, M. Abdel-Hafiez, J. Seidel, R. Hüttl, A.U.B. Wolter, K. Bohmhammel, F. Mertens, Heat capacity (C_p) and entropy of olivine-type $LiFePO_4$ in the temperature range (2 to 773)K, J. Chem. Thermodyn. 85 (2015) 77–85.
[26] H.Y. Bai, J.L. Luo, D. Jin, Particle size and interfacial effect on the specific heat of nanocrystalline Fe, J. Appl. Phys. 79 (1996) 361–364.
[27] L. Li, L.P. Li, X.J. Wang, G.S. Li, Understanding of the finite size effects on lattice vibrations and electronic transitions of nano α-Fe_2O_3, J. Phys. Chem. B 109 (2005) 17151–17156.
[28] F. Jones, A.L. Rohl, J.B. Farrow, W.V. Bronswijk, Molecular modeling of water adsorption on hematite, Phys. Chem. Chem. Phys. 2 (2000) 3209–3216.
[29] J.C. Lashley, M.F. Hundley, A. Migliori, J.L. Sarrao, P.G. Pagliuso, T.W. Darling, M. Jaime, J.C. Cooley, W.L. Hults, L. Morales, Critical examination of heat capacity measurements made on a Quantum Design physical property measurement system, Cryogenics 43 (2003) 369–378.
[30] C.A. Kennedy, M. Stancescu, R.A. Marriott, M.A. White, Recommendations for accurate heat capacity measurements using a Quantum Design physical property measurement system, Cryogenics 47 (2007) 107–112.
[31] Q. Shi, C.L. Snow, J. Boerio-Goates, B.F. Woodfield, Accurate heat capacity measurements on powdered samples using a quantum Design physical property measurement system, J. Chem. Thermodyn. 42 (2010) 1107–1115.
[32] W.H. Luo, W.Y. Hu, S.F. Xiao, Size effect on the thermodynamic properties of silver nanoparticles, J. Phys. Chem. C 112 (2008) 2359–2369.
[33] E.F. Westrum, A.F. Beale, Heat capacities and chemical thermodynamics of cerium(III) fluoride and cerium(IV) oxide from 5 K to 300 K, Indian, J. Chem. Appl. 29 (1961) 67–70.
[34] L. Wang, Z.C. Tan, S.H. Meng, D.B. Liang, J.H. Li, Enhancement of molar heat capacity of nanostructured Al_2O_3, J. Nano Res. 3 (2001) 483–487.
[35] T. Feng, L. Li, Q. Shi, Heat capacity and thermodynamic functions of TiO_2 (B) nanowires, J. Chem. Thermodyn. 93 (2016) 45–51.
[36] C.L. Snow, K.I. Lilova, A.V. Radha, Heat capacity and thermodynamics of a synthetic two-line ferrihydrite, $FeOOH{\cdot}0.027H_2O$, J. Chem. Thermodyn. 58 (2013) 307–314.
[37] E.S.R. Gopal, Specific Heats at Low Temperatures, Springer Science & Business Media, 2012.
[38] Q. Shi, L. Zhang, M.E. Schlesinger, Low temperature heat capacity study of $FePO_4$, and $Fe_3(P_2O_7)_2$, J. Chem. Thermodyn. 62 (2013) 35–42.
[39] Z.X. Huang, P. Thomson, S.L. Di, Lattice contractions of a nanoparticle due to the surface tension: a model of elasticity, J. Phys. Chem. Solid. 68 (2007) 530–535.
[40] J.M. Schliesser, S.J. Smith, G. Li, Heat capacity and thermodynamic functions of nano-TiO_2, rutile in relation to bulk-TiO_2 Rutile, J. Chem. Thermodyn. 81 (2015) 311–322.
[41] P. Patnaik, Handbook of Inorganic Chemicals, McGraw-Hill, New York, 2003, p. 529.
[42] N.Y. Sdobnyakov, V.M. Samsonov, On the size dependence of surface tension in the temperature range from melting point to critical point, Cent. Eur. J. Phys. 3 (2005) 247–257.
[43] H.F. Tang, Z.Y. Huang, M. Xiao, Effects of particle size and temperature on surface thermodynamic functions of cubic nano-Cu_2O, Acta Phys. Chim. Sin. 32 (2016) 2678–2684.